Original Article

Intra-abdominal temperature variation during hyperthermic intraperitoneal chemotherapy evaluated via computational fluid dynamics modeling

Olivia S. Cooney[1#], Dylan A. Goodin[1#], Tyler J. Mouw[2], Robert C. G. Martin[2], Hermann B. Frieboes[1,3,4]

[1]Department of Bioengineering, University of Louisville, Louisville, KY, USA; [2]Department of Surgery, University of Louisville, Louisville, KY, USA; [3]James Graham Brown Cancer Center, University of Louisville, Louisville, KY, USA; [4]Center for Predictive Medicine, University of Louisville, Louisville, KY, USA

Contributions: (I) Conception and design: All authors; (II) Administrative support: RCG Martin, HB Frieboes; (III) Provision of study materials or patients: TJ Mouw, RCG Martin; (IV) Collection and assembly of data: OS Cooney, DA Goodin; (V) Data analysis and interpretation: All authors; (VI) Manuscript writing: All authors; (VII) Final approval of manuscript: All authors.

[#]These authors contributed equally to this work.

Correspondence to: Hermann B. Frieboes, PhD. Department of Bioengineering, University of Louisville, Lutz Hall 419, Louisville, KY 40292, USA; James Graham Brown Cancer Center, University of Louisville, Louisville, KY, USA; Center for Predictive Medicine, University of Louisville, Louisville, KY, USA. Email: hbfrie01@louisville.edu.

Background: Hyperthermic intraperitoneal chemotherapy (HIPEC) targets intraperitoneal tumors with heated drug solutions via catheters inserted into the peritoneal space. Although studies have focused on clinical outcomes, the flow dynamics at specific intra-abdominal locations at-risk of harboring malignant cells remain poorly understood but are likely to impact the drug pharmacokinetics. Consequently, optimal protocols remain uncertain, with efficacy critically dependent on drug temperature and flow rate. This study tested the hypothesis that fluid flow dynamics at specific at-risk locations could be evaluated via a computational fluid dynamics (CFD) model of closed HIPEC in a simulated human abdominal cavity, with the goal to enable protocol optimization.

Methods: A computer-aided-design (CAD) model of a human intraperitoneal cavity (30 L) was coupled with computational fluid dynamics analysis. The tested HIPEC cycle parameters included catheter position and flow rates. The cavity was subjected to forward (superior to inferior flow) or reverse flow directions at 800 or 1,120 cc/min through four catheters, two as inlets and two as outlets, placed in upper and lower abdominal positions (net fluid volume: 18.5 L). Probes to measure temperature and flow were simulated between small and large bowels, inferior to small bowel mesentery, next to duodenum, superior to liver, superior to fundus, posterior to stomach, and posterior to liver.

Results: The simulations highlight heterogeneity in temperatures and flow that may occur during HIPEC at particular at-risk locations as a function of chemotherapy flow rate and direction. Temperature and fluid flow over the course of 90 min respectively varied from 0.93 K and <0.001 m/s inferior to small bowel mesentery (800 cc/min forward flow) to 3.6 K and 0.01 m/s next to the duodenum (either 800 or 1,120 cc/min forward flow). The results further suggest that monitoring outflow temperature may be inadequate for assessing HIPEC performance at at-risk locations.

Conclusions: Without intra-abdominal temperature monitoring at at-risk locations, it may be unfeasible to determine whether target temperatures and temperature homogeneity are being achieved during HIPEC. This work demonstrates that computational analysis offers the capability to monitor intra-abdominal locations at-risk of suboptimal heating and fluid flow given specific HIPEC parameters, and represents a first step towards designing efficacious tumor targeting during HIPEC.

Keywords: Hyperthermic intraperitoneal chemotherapy (HIPEC); computational modeling; simulation; fluid dynamics

Submitted May 10, 2024. Accepted for publication Jul 18, 2024. Published online Aug 28, 2024.
doi: 10.21037/jgo-24-352
View this article at: https://dx.doi.org/10.21037/jgo-24-352

Introduction

Background

Hyperthermic intraperitoneal chemotherapy (HIPEC) is a treatment indicated for peritoneal carcinomatosis. While HIPEC is only offered at select hospitals, it is estimated that up to 40,000 patients are annually considered eligible for cyto-reductive surgery (CRS) plus HIPEC in the U.S. (1). HIPEC is considered for managing digestive tract (2) as well as ovarian (3,4) cancers. During HIPEC, a heated chemotherapy solution is circulated through the abdomen for a period, typically 1–2 hours, to treat tumor cells post CRS (5,6). HIPEC may be advantageous over systemically administered bolus injection by directly exposing cancer cells disseminated within the abdominal cavity to cytotoxic doses without relying on diffusion from the vascular network.

The chemotherapy can be applied directly while the abdomen is surgically opened after the CRS (7) or via catheters following abdominal closure (8). Closed HIPEC involves filling the abdominal cavity with a solution heated to 43–45 ℃ containing a chemotherapy drug such as mitomycin C or cisplatin, which is then cycled through the abdomen using inlet and outlet catheters in series with a pump (9-11). Regardless of approach, it is critical for the success of HIPEC that the peritoneal surfaces be exposed equally at elevated temperatures over the course of the procedure, typically ≥39 ℃, while avoiding healthy tissue over-exposure or higher temperatures, e.g., ~43 ℃ (9), so that every cancer cell disseminated in the abdomen is subjected to high temperature and cytotoxic drug levels.

Highlight box

Key findings

- This study implemented a computational fluid dynamics (CFD)-based model of the abdominal cavity and associated key organs to evaluate the fluid dynamics at specific at-risk locations where tumor cells may be under-exposed to drug or higher temperature during HIPEC. Simulations quantitatively evaluated temperature changes and fluid velocities as a function of cycle parameters. Even with the best combination of parameters tested, several intra-abdominal locations had not yet reached the target temperature by 30 min. The results further suggest that monitoring outflow temperature may be inadequate for assessing hyperthermic intraperitoneal chemotherapy (HIPEC) performance at at-risk locations.

What is known and what is new?

- Since chemotherapy performance during HIPEC improves with increasing temperature, intra-abdominal thermal heterogeneity could yield uneven therapeutic performance. This study implemented a CFD model as a tool to quantitatively evaluate the flow of drug within the abdominal cavity during closed HIPEC, enabling detailed evaluation of fluid flow dynamics at at-risk locations.

What is the implication, and what should change now?

- Computational modeling can quantitatively evaluate HIPEC performance at at-risk locations to enable procedure optimization without solely relying on outflow temperature. Expanding the modeling capabilities to explore alternative catheter arrangements in addition to other cycle parameters may allow for designing techniques that produce rapid equilibration of temperature across all at-risk locations, with the goal to maximize tissue exposure times while minimizing overall procedure durations.

Rationale and knowledge gap

While studies have established concepts such as synergism between chemotherapy and hyperthermia (12) and the degree of tumor tissue penetration (13), relatively little is understood about how flow influences temperature homogeneity and drug distribution. Recent literature highlights that HIPEC efficacy remains controversial, due in part to variation of key cycle parameters in clinical practice (14-16), including temperature, volume, flow rate, and duration. A comprehensive understanding of these parameters is a prerequisite to developing a standardized high-quality HIPEC technique.

Objective

An analysis involving a computational fluid dynamics (CFD) simulation offers a means to evaluate the effect of therapy parameters such as abdominal local temperatures and flow rates on treatment efficacy. CFD has been extensively applied to study flow in organs and physiological systems, including cardiovascular function (17,18), aortic (19) and brain aneurysms (20,21), stomach food digestion (22), hepatic microcirculation (23), lung airflow and aerosol

deposition (24), maternal-fetal umbilical cord heat and blood exchange (25), and intraperitoneal cisplatin penetration into mouse tumor nodules (26). CFD has been used to simulate drug penetration into tumor nodules during open HIPEC, simulating fluid flow in a single direction (13), finding that moderate flow velocities between 0.01 and 1 m/s in the intraperitoneal cavity were optimal for cisplatin delivery. Recently, a treatment planning software was developed to evaluate the impact of treatment strategies on thermal and drug distributions during closed HIPEC, with simulation results compared to clinical measurements (27). However, the contribution of catheter flow rate and direction at specific locations at-risk of suboptimal drug and temperature exposure. especially during closed HIPEC, would benefit from further analysis. This study implements a CFD model to simulate the flow of solution within the abdominal cavity during closed HIPEC, enabling evaluation of fluid flow dynamics at specific at-risk locations. The longer term objective is to develop a platform for personalized HIPEC evaluation of drug delivery from a kinetic and dynamic viewpoint.

Methods

Design of abdominal cavity

To represent a human intra-abdominal cavity undergoing HIPEC, an abdominal intraperitoneal space (volume: 30 L) was designed in SOLIDWORKS (V.2021, Dassault Systèmes, Waltham, MA), software for 3D computer-aided design (CAD). This model contained stomach, liver, transverse colon, transverse colon mesentery (TCM), small bowel, and small bowel mesentery. Other organs and tissue were not modeled, as they are either removed during surgery or do not occupy the intraperitoneal space. Ansys Fluent (Version 2022 R1, Ansys, Inc. Canonsburg, PA, USA), was used to complete the CFD simulation within the modeled anatomy. The model was implemented as a 3D cavity shape resembling the axial, sagittal, and coronal planes of an adult abdomen. Because chemotherapeutics in HIPEC, such as cisplatin (28), are commonly diluted in a water-based solution such as 1.5% dextrose isotonic peritoneal dialysis solution or saline (29,30), water was chosen as the simulated fluid. Accordingly, the cavity was modeled as an enclosure filled with water (net fluid volume: 18.5 L) assumed to contain rigid, unmovable organs. In doing so, it was further assumed that HIPEC chemotherapy negligibly affects the fluid dynamics of the interstitial media. For simplicity, effects of gravitational forces and the viscoelastic properties of abdominal organs (31) were neglected and will be considered in future work. Material properties for water were provided in the Ansys Fluent Fluid Library. Organ material properties were obtained from a tissue property database provided by IT'IS Foundation (32). Material properties are in Table S1. Cell zone conditions for liver, small bowel and mesentery, liver, and transverse colon were set to solid.

Design and placement of catheters and intra-abdominal probes

Catheters were simulated at the upper and lower regions of the peritoneal cavity. Two catheters at each portion were inserted to simulate the two-pronged Y-shaped catheter used in clinical practice (10). To represent each catheter, 0.4" diameter holes (1.016 cm) were simulated through the abdominal cavity with tubes extending 3.00" (7.62 cm) into the cavity. All catheters were assumed to have the same dimensions. Catheters were given material properties of silicone rubber with a density of 1,049 kg/m^3, specific heat of 1050 J/(kg·K), and thermal conductivity of 1.9 W/(m·K) (33). To investigate heterogeneity in fluid flow within the abdominal cavity, temperature and flow were measured in Ansys Fluent at seven at-risk locations: between small and large bowels, inferior to small bowel mesentery, next to duodenum, superior to liver, superior to fundus, posterior to stomach, and posterior to liver. To calculate variation in temperature and velocity magnitude, infinitesimally sized ("rake") probes (n=3, evenly spaced) were used at each location.

Characterization of fluid flow

To analyze the effect of flow rate and direction, 800 cc/min (0.0133 kg/s) and a 40% increase in flow (1,120 cc/min or 0.01867 kg/s) were evaluated with either upper to lower (forward) or lower to upper (reverse) flow directions, for a total of four cases. These numbers are approximate given that the density of liquid water decreases as temperature increases at constant pressure. To determine flow characteristics, the Reynolds number was calculated as in Appendix 1.

Model of fluid flow

Because fluid flow is assumed incompressible, a pressure-

based solver was applied over a density-based solver that is typically used to evaluate high-speed compressible flow (34). To improve the robustness of transient solutions, pressure and velocity were coupled. Velocity and pressure were solved via momentum and pressure-based continuity equations, respectively (35). Since flow may not be distributed equally across the two outlet catheters and thus potentially be non-laminar (Re >2,000), the flow was modelled using the SST k-ω model, the default k-ω model in Ansys Fluent (35). SST k-ω has also been found to better replicate blood flow patterns than laminar flow models, as well as k-ε RNG and standard k-ω models (36). The model of fluid flow is further described in Appendix 1.

Model of heat transport

Fluid energy was modeled using the conservation of energy equation in (10) and solved using the pressure-based solver. The model for heat transport is further described in Appendix 1.

Initial and boundary conditions

The circular catheter cross-sectional surfaces inside the cavity served as the boundary conditions for fluid inflow and outflow. Fluid inlets were placed at either the upper abdominal region (forward flow) with outlets in the lower region or with inlets in the lower region (reverse flow) and outlets in the upper region. The inlet boundary condition was set to a mass-flow with baseline flow rate, provided by the collaborating surgeon, of 0.0133 kg/s (800 cc/min), with all other settings at default values. The outlet boundary condition was set to pressure outlet using default settings. To represent a slight decrease in temperature normally found in anesthetized patients (37), body fluid within the cavity and organs were set to 309.15 K (36 ℃). Inlet fluid temperature was set to 316.15 K (43 ℃). Based on prior studies, target tissue temperature was set at 39 ℃ (38). Heat transfer to and from the catheters was assumed to be negligible in this study and was not modeled. The abdominal cavity was treated as the boundary of the system with a Dirichlet boundary condition of 309.15 K. All other initial condition settings were left at default values.

Numerical methods

Double precision mode was used for the CFD simulations. SIMPLEC (SIMPLE-Consistent) with default settings was used to improve the convergence of pressure-velocity coupling (35). Convergence criteria for each time step was set to 1E–2 for continuity, 1E–4 for velocity components, k, and ω, and 1E–6 for energy. Because HIPEC is normally performed for 1 to 2 hours (5,6), time was set to run for 90 simulated minutes.

Statistical analysis

All statistical analyses comparing simulation results were performed using Welch's *t*-test with Bonferroni correction applied for multiple hypothesis testing ($P_{adj} \leq 0.05$).

Results

Simulation of abdominal cavity

The completed SOLIDWORKS design is shown from anterior (*Figure 1A*) and isometric (*Figure 1B*) views. Dimensions of the abdominal cavity and organs simulated are specified in Table S2. Y-shaped catheters were placed in upper and lower regions in the abdominal cavity (*Figure 1C*) to match clinical practice at our institution (10). To measure flow velocity and temperature at different locations within the simulated abdominal cavity, infinitesimally sized ("rake") probes (n=3) were added to seven at-risk locations as shown in *Figure 2*. Grid and time step independence were ensured as described in Appendix 1.

Effect of fluid rate and direction on intra-abdominal temperature change

To evaluate the effect of fluid flow on temperature change at the different intra-abdominal locations, fluid entered the abdominal cavity at either 800 or 1,120 cc/min in either forward (upper to lower) or reverse (lower to upper) directions. The average change in fluid temperature with respect to time within the cavity at each probe location for each of these conditions is shown in *Figure 3* at 10 min intervals, showing that temperature had fairly stabilized by 30 min for all cases. Almost all probes experienced a monotonic increase in temperature that steadily plateaued over the course of the simulation. Unsurprisingly, standard deviations decreased as average temperature change decreased. Probe 2 (inferior to small bowel mesentery) was secluded from forward fluid flow, being blocked by the TCM and had a delayed temperature response at 800 cc/min (*Figure 3A*). However, temperature change over time at

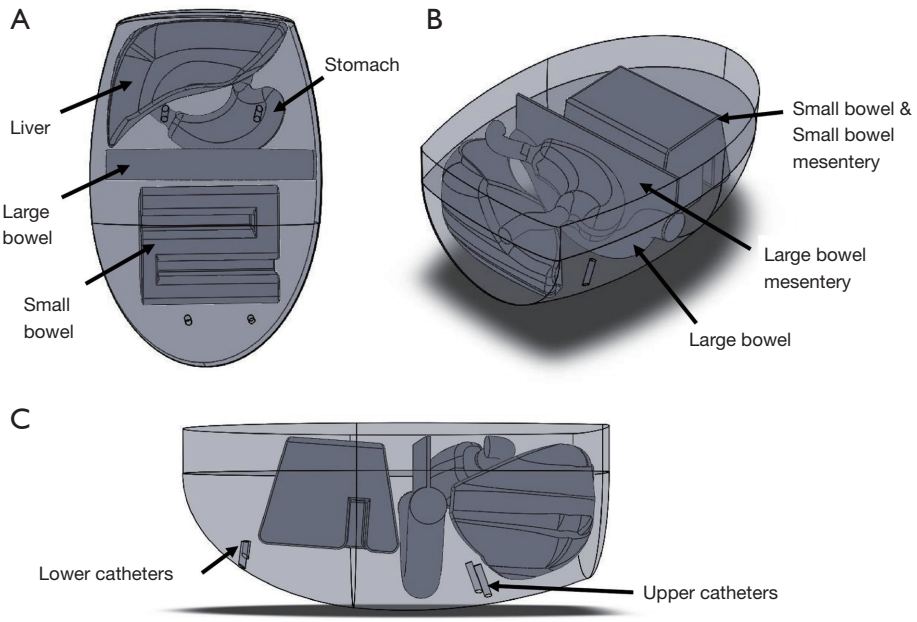

Figure 1 Abdominal cavity simulated in SOLIDWORKS. (A) Anterior view; (B) isometric view; (C) upper and lower positioning of catheters in the cavity (dual inlets and outlets were used to represent Y-shaped catheters).

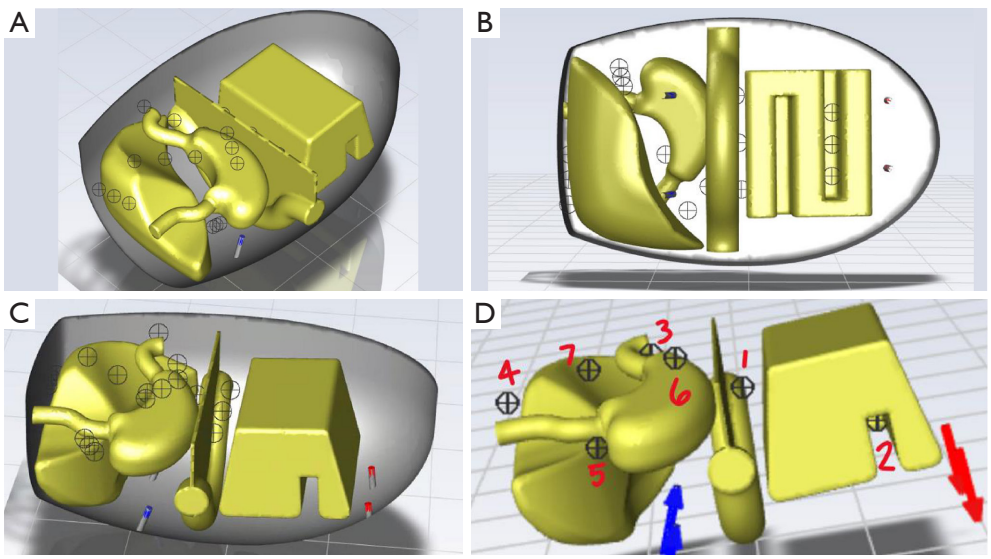

Figure 2 Placement of probes at seven at-risk locations within the simulated abdominal cavity [each probe is a "rake" (n=3, crosshair symbols)]. (A) Isometric view; (B) anterior view; (C) posterior view showing upper (blue) and lower (red) catheters; (D) locations of probe "rakes" (bolded crosshair symbols): 1: between small and large bowels; 2: inferior to small bowel mesentery; 3: next to duodenum; 4: superior to liver; 5: superior to fundus; 6; posterior to stomach; 7: posterior to liver. As an example, inlet flow is shown by blue arrows and outlet flow is denoted by red arrows.

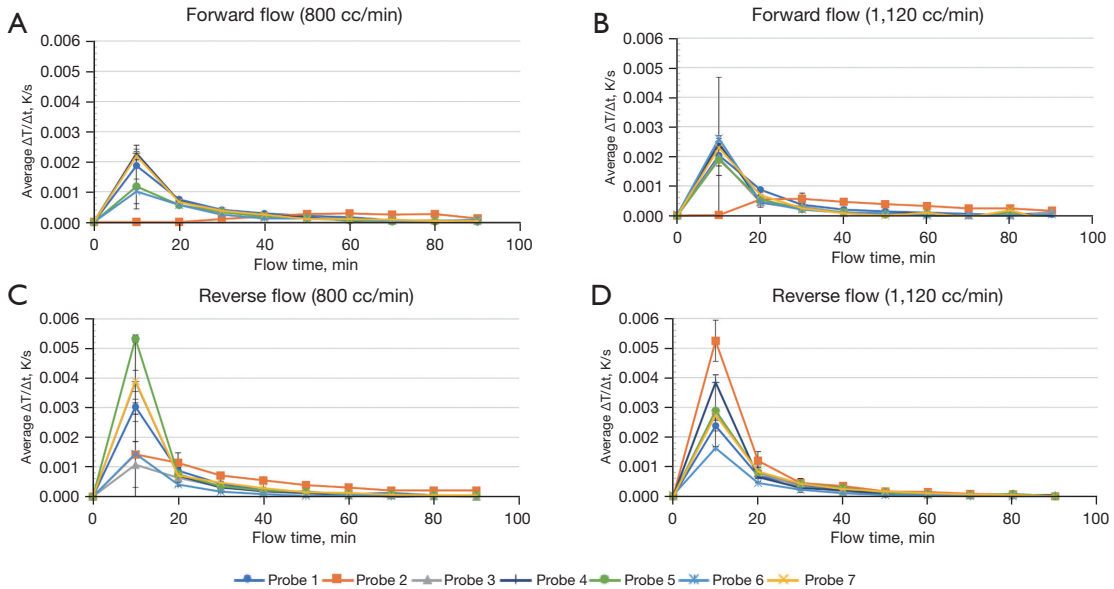

Figure 3 Average change in temperature (T) with respect to time (t) within the cavity at each probe location. (A) Forward flow (upper inlet) at baseline 800 cc/min; (B) forward flow at 1,120 cc/min representing a 40% increase from baseline; (C) reverse flow (lower inlet) at 800 cc/min; (D) reverse flow at 1,120 cc/min. Probe locations; 1: between small and large bowels; 2: inferior to small bowel mesentery; 3: next to duodenum; 4: superior to liver; 5: superior to fundus; 6; posterior to stomach; 7: posterior to liver. Error bars: standard deviation; each probe was represented as a "rake" (n=3) in Ansys Fluent.

Probe 2 was significantly higher under reverse flow relative to forward flow at certain times of the procedure at both 800 cc/min (1.83E−4 *vs.* 5.49E−4 K/s at t=40 min; P_{adj} =0.020) and 1,120 cc/min (1.63E−4 *vs.* 0.00 K/s at t=90 min; P_{adj}=0.042), highlighting the heterogeneity of temperature at particular locations and their dependence on fluid flow direction.

Temperatures at at-risk locations

To evaluate temperature values at the various at-risk locations, flow rates and fluid temperatures were recorded for each of the four flow cases. Temperatures were largely uniform for most probed locations with both 800 and 1,120 cc/min forward fluid flow (*Figure 4A*,*4B*, respectively), rising from 309.15 K initial condition to ~312 K in both cases by 90 min. However, 800 cc/min forward flow only increased temperatures at Probe 2 (inferior to small bowel mesentery) by ~1 K due to obstruction by the TCM. Temperatures at Probe 2 under forward flow were significantly lower compared to other probes by t=90 min in both 800 cc/min (P_{adj}≤0.05) and 1,120 cc/min (P_{adj}≤0.05) cases. This trend was absent in reverse flow for both 800 cc/min (*Figure 4C*) and 1,120 cc/min cases (*Figure 4D*), with Probe 2 temperatures responding, and reaching similar temperatures to the other probes by 20 and 10 min, respectively. Average temperature of Probe 3 (next to duodenum) trended ~1 K lower than the other probes under reverse flow, suggesting that heating was not uniformly occurring during the simulated procedure. The time to reach the target temperature and the maximum temperature reached at each probe location are summarized in *Table 1*. The time to target temperature for each probe differed significantly between cycle conditions, overall ranging from 16.28 to 86.44 min between the probes and conditions tested, and with some probes failing to reach it. Positioning the inflow in reverse configuration decreased the time for Probes 1, 2, and 4 to reach the target temperature. As expected, a higher flow rate also decreased this time for all probes. These data further show that although some probes reached the target temperature within the course of the procedure, they would be exposed to it for <60 min. In contrast, the outflow did not necessarily reflect the conditions at the probes, reaching 311.65±0.18 K by 90 min for all the configurations tested.

Differences in temperature at 90 min under forward and reverse flow at each probe are highlighted for 800 and

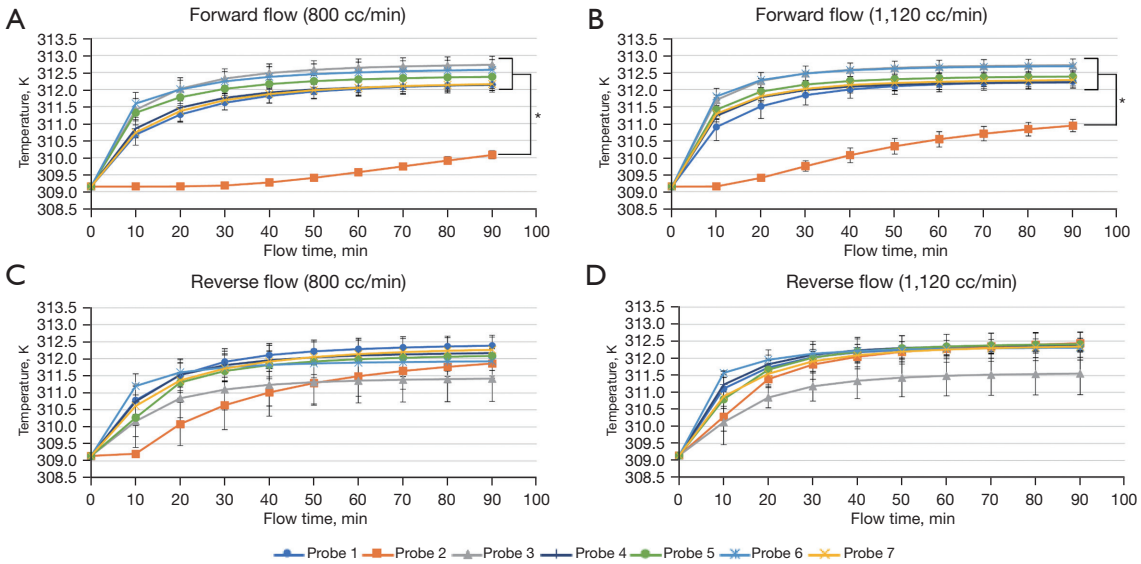

Figure 4 Temperatures in the abdominal cavity at each probe location measured every 10 min for 90 min of flow time. (A) Fluid temperature during forward (upper inlet) flow at 800 cc/min flow; (B) fluid temperature during forward flow at 1,120 cc/min flow; (C) fluid temperature during reverse (lower inlet) flow at 800 cc/min flow; (D) fluid temperature during reverse flow at 1,120 cc/min flow. Probe locations; 1: between small and large bowels; 2: inferior to small bowel mesentery; 3: next to duodenum; 4: superior to liver; 5: superior to fundus; 6; posterior to stomach; 7: posterior to liver. Error bars: standard deviation; each probe was represented as a "rake" (n=3) in Ansys Fluent; *, $P_{adj} \leq 0.05$.

Table 1 Temperature assessment during simulated HIPEC

Probe	Forward 800 cc/min		Forward 1,120 cc/min		Reverse 800 cc/min		Reverse 1,120 cc/min	
	Max Temp (K)	Time to α (min)	Max Temp (K)	Time to α (min)	Max Temp (K)	Time to α (min)	Max Temp (K)	Time to α (min)
1	312.14 (0.22)	[49.20]	312.23 (0.20)	59.66	312.39 (0.25)	42.95	312.35 (0.41)	37.14
2	310.08 (0.12)	NR	310.94 (0.18)	NR	311.87 (0.43)	[66.83]	312.44 (0.14)	46.60
3	312.73 (0.15)	23.44	312.72 (0.18)	17.15	311.42 (0.67)	NR	311.56 (0.63)	[75.58]
4	312.14 (0.16)	[50.02]	312.21 (0.17)	54.08	312.17 (0.52)	77.90	312.40 (0.37)	32.46
5	312.37 (0.35)	38.99	312.38 (0.28)	30.24	312.08 (0.06)	NR	312.42 (0.04)	36.28
6	312.58 (0.40)	25.50	312.68 (0.06)	16.28	311.93 (0.43)	[30.60]	312.32 (0.10)	30.95
7	312.16 (0.19)	86.44	312.28 (0.23)	42.68	312.27 (0.12)	61.79	312.35 (0.12)	44.67

For each configuration, shown are maximum average temperature attained for each probe during the simulated procedure [average (SD)] and the time for probe average temperature to reach ≥ α (where α =312.15 K). Cases for which average temperature failed to reach ≥ α but (average temperature + SD) ≥ α within the duration of the procedure (90 min), the time for (average temperature + SD) ≥ α is shown in square brackets. All other cases are denoted by "NR" (temperature not reached). Probe locations; 1: between small and large bowels; 2: inferior to small bowel mesentery; 3: next to duodenum; 4: superior to liver; 5: superior to fundus; 6; posterior to stomach; 7: posterior to liver. Each probe was represented as a "rake" (n=3) in Ansys Fluent. HIPEC, hyperthermic intraperitoneal chemotherapy; SD, standard deviation.

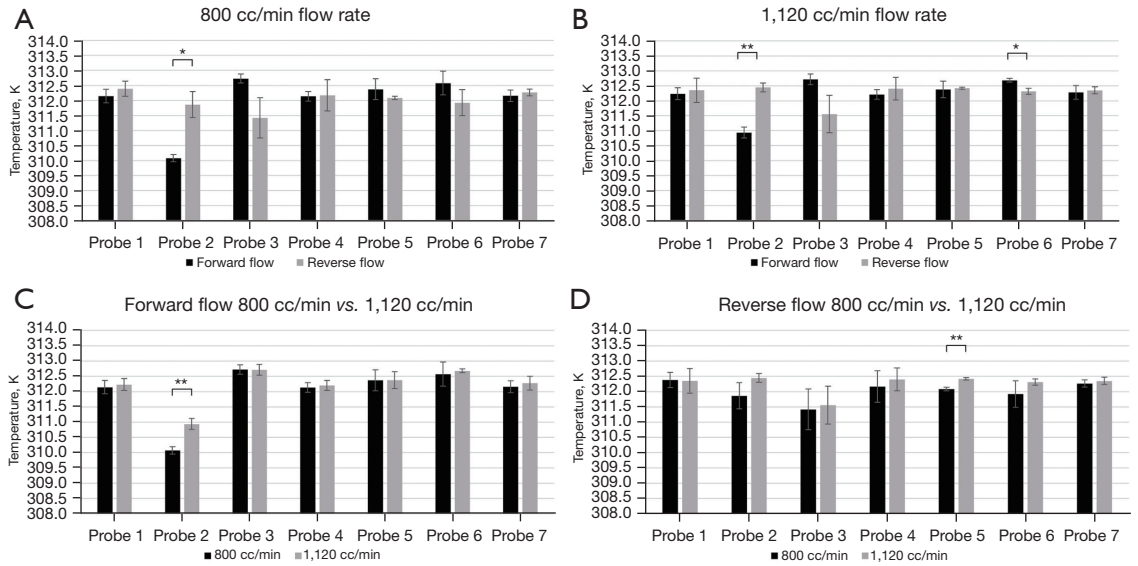

Figure 5 Temperatures in the abdominal cavity at each probe location at 90 min of flow time. (A) Temperatures compared between forward (upper inlet) and reverse (lower inlet) flow at 800 cc/min flow rate; (B) temperatures compared between forward and reverse flow at 1,120 cc/min flow rate; (C) temperatures compared between 800 and 1,120 cc/min flow rates under forward flow; (D) temperatures compared between 800 and 1,120 cc/min flow rates under reverse flow. Probe locations; 1: between small and large bowels; 2: inferior to small bowel mesentery; 3: next to duodenum; 4: superior to liver; 5: superior to fundus; 6; posterior to stomach; 7: posterior to liver. Error bars: standard deviation; each probe was represented as a "rake" (n=3) in Ansys Fluent; *, P≤0.05; **, P≤0.01.

1,120 cc/min in *Figure 5A*,*5B*, respectively. For comparison, *Figure 5C*,*5D* quantify how probe temperatures at 90 min under forward and reverse flow, respectively, were affected by changing flow rate from 800 to 1,120 cc/min. The largest difference between temperature and fluid flow was between Probe 2 under 800 cc/min forward flow configuration (0.93 K and 1E−5 m/s) and Probe 3 (3.6 K and 0.01 m/s) under both 800 and 1,120 cc/min in forward flow (*Figure 5C*). This analysis shows that the location at Probe 2 benefited from reverse flow irrespective of flow rate and from higher flow during forward flow. The location at Probe 6 (posterior to stomach) benefited from forward flow at 1,120 cc/min, while the location at Probe 5 (superior to fundus) benefited from higher flow under reverse flow.

Fluid velocities at at-risk locations

To investigate differences in fluid flow as a function of intra-abdominal location, velocity magnitudes were measured at each probe. The magnitudes for both 800 cc/min (*Figure 6A*) and 1,120 cc/min (*Figure 6B*) consistently trended higher for forward flow at 90 min compared to reverse flow. Probe 2, being secluded from fluid flow by the TCM, experienced a low fluid velocity for all flow cases (<0.001 m/s). Due to its proximity to inlets during forward flow and the large bowel mesentery relative to other probe locations, velocity magnitude at Probe 3 (next to duodenum) under forward flow trended higher than with reverse flow. However, variation for forward fluid flow was large for both 800 cc/min (8.5E−3 m/s) and 1,120 cc/min (1.1E−2 m/s), indicating that selection of flow entrance rate and direction may yield heterogeneous temperature and velocity magnitude responses during HIPEC at multiple locations. Velocity magnitude at Probe 4 (superior to liver) was significantly higher in forward flow compared to reverse flow at both 800 cc/min (1.20E−3 *vs.* 5.06E−4 m/s; P=0.028) and 1,120 cc/min (2.46E−3 *vs.* 7.62E−4 m/s; P=0.018). Probe 5 (superior to fundus) at 800 cc/min flow rate had higher velocity magnitude in forward (2.23E−3 m/s) *vs.* reverse (5.89E−4 m/s) conditions (P=2E−4). Velocity magnitude at Probe 6 (posterior to stomach) was significantly higher at 1,120 cc/min (1.04E−2 m/s *vs.* 4.51E−3 m/s; P=0.011). Lastly, velocity magnitudes at Probe 1 (between small and large bowels) and Probe 7 (posterior to liver) did not significantly differ under changing flow directions.

With the exception of Probe 4 (superior to liver)

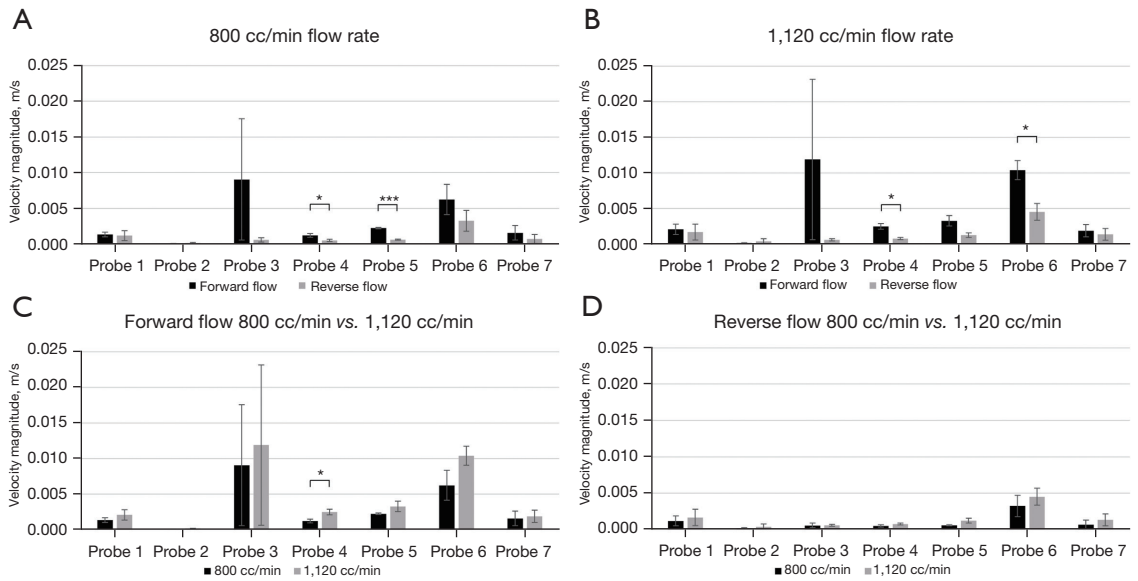

Figure 6 Velocity magnitudes in the abdominal cavity at each probe location at 90 min of flow time. (A) Velocity magnitudes compared between forward (upper inlet) and reverse (lower inlet) flow at 800 cc/min flow rate; (B) velocity magnitudes compared between forward and reverse flow at 1,120 cc/min flow rate; (C) velocity magnitudes compared between 800 and 1,120 cc/min flow rates under forward flow (D) velocity magnitudes compared between 800 and 1,120 cc/min flow rates under reverse flow. Probe locations; 1: between small and large bowels; 2: inferior to small bowel mesentery; 3: next to duodenum; 4: superior to liver; 5: superior to fundus; 6; posterior to stomach; 7: posterior to liver. Error bars: standard deviation; each probe was represented as a "rake" (n=3) in Ansys Fluent; *P≤0.05; ***P≤0.001.

under forward flow (P=0.017), velocity magnitude did not significantly differ for the various locations between 800 and 1,120 cc/min cases under forward (*Figure 6C*) and reverse (*Figure 6D*) flows. The potential heterogeneity in temperature induced by the flow rate and direction at the various at-risk locations is summarized in *Figure 7*, showing that change in flow rate yielded significant differences in temperatures at Probe 3 (next to duodenum) and Probe 5 (superior to fundus) (*Figure 7A*) and in flow velocities at Probe 4 (superior to liver) and Probe 6 (posterior to stomach) (*Figure 7B*). In comparison, change in flow direction yielded significant difference in temperature at Probe 6 (*Figure 7C*) and in flow velocities at Probe 4 and Probe 6 (*Figure 7D*).

Comparison to clinical data

To contextualize the simulation results with current literature, outlet temperature results were compared to a retrospective study of 1,200 patients (10) completed in Guangzhou, China. In that study, 3 sessions of HIPEC were performed at flow rates of 450 to 600 cc/min, with inlet fluid temperature of 43 ℃, and with each session lasting 90 min, with inlet catheters in upper abdominal position. Chemotherapy drug and dosage were selected based on the primary tumor and the patient's body weight (10). Outlet temperatures were recorded at procedure start and at 30 min intervals up to 120 min, with the procedure ending at t=90 min. Fluid temperature at outlets rose from 39.6 (SD 0.7 ℃) at procedure start to 42.0 ℃ (SD 0.1 ℃) after 90 min. In this study's CFD model, using forward direction flow (upper inlets) and 525 cc/min flow rate with inlet fluid temperature of 43 ℃ for 90 min, the outlet temperature was recorded as 38.06 ℃ (SD 0.58 ℃) with an absolute difference of 3.94 ℃ at t=90 min from the data in (10). Of note, flow rate varied between patients in (10), whereas CFD flow rates were held constant in this study.

Discussion

Key findings

HIPEC is a treatment strategy for peritoneal carcinomatosis that is applied in a consistently unstandardized manner. This study implemented a CFD-based model of the abdominal cavity and associated key organs to evaluate the

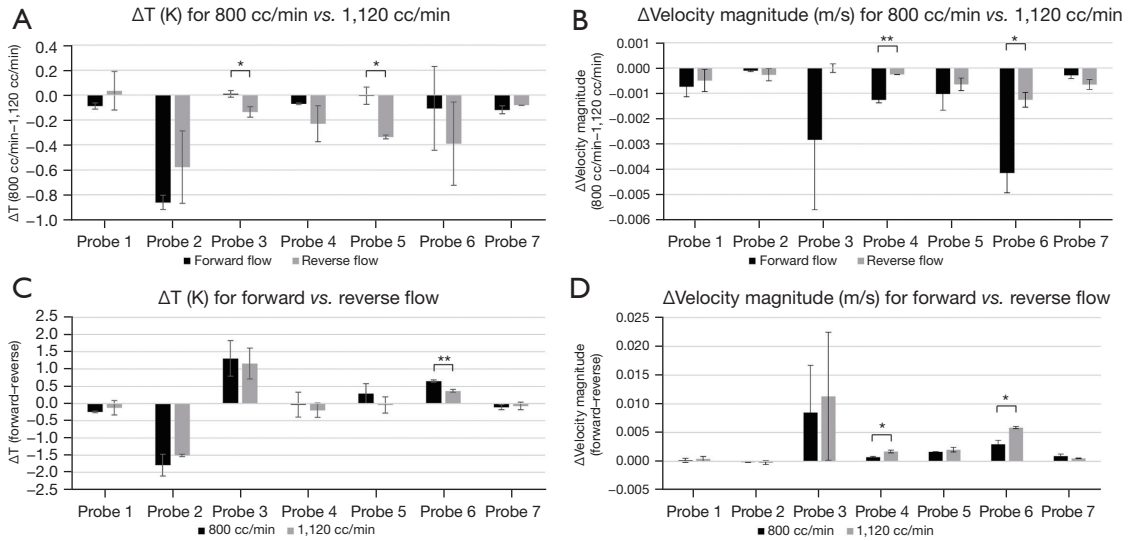

Figure 7 Difference in fluid temperatures (ΔT) and in velocity magnitudes (ΔV) at each probe location at 90 min of flow time. (A) Temperature difference between 800 and 1,120 cc/min flow rates based on flow direction; (B) difference in velocity magnitude between 800 and 1,120 cc/min flow rates based on flow direction; (C) temperature difference between forward (upper inlet) and reverse (lower inlet) flow based on flow rate; (D) difference in velocity magnitude between forward and reverse flow based on flow rate. Probe locations; 1: between small and large bowels; 2: inferior to small bowel mesentery; 3: next to duodenum; 4: superior to liver; 5: superior to fundus; 6; posterior to stomach; 7: posterior to liver. Error bars: standard deviation; each probe was represented as a "rake" (n=3) in Ansys Fluent; *, P≤0.05; **, P≤0.01.

effect of therapy parameters at specific at-risk locations where tumor cells may be under-exposed to drug or higher temperature. Two flow rates (800 and 1,120 cc/min) and two flow directions were simulated to evaluate temperatures and flow at these locations. Simulations show that temperature and fluid flow over the course of the procedure varied from 0.93 K and <0.001 m/s inferior to small bowel mesentery (800 cc/min forward flow) to 3.6 K and 0.01 m/s next to the duodenum (either 800 or 1,120 cc/min forward flow). The results suggest that monitoring outflow temperature may be inadequate for assessing HIPEC performance at at-risk locations.

Strengths and limitations

The model presented in this study enables monitoring of temperature changes and fluid velocities at intra-abdominal at-risk locations as a function of HIPEC procedure parameters, which is not feasible by only monitoring the outflow temperature. The flexibility of the modeling approach enables investigating parameters to minimize flow and temperature heterogeneity at at-risk locations to maximize therapeutic efficacy. This study used 39.0 ℃ as the minimum target temperature to define "successful" treatment during HIPEC. It is unlikely that synergy occurs in such a binary fashion around a specific temperature, but instead there is a spectrum of synergy that occurs with increasing temperature (38). Additionally, there is no clear consensus on the minimum temperature needed (38-40). A strength of this model is the continuous monitoring of endpoints as the cycle progresses. allowing for the assessment of success for any particular temperature threshold.

The simulations treated organs as rigid bodies with no viscoelastic properties. Abdominal organs are known to behave viscoelastically (31), which may affect fluid flow and, by extension, heat distribution in the abdominal cavity. It is unclear, however, whether non-rigid organs would improve or impede the fluid flow and associated heat transport at at-risk locations. The catheter inflow and outflow were limited in this study to the anterior of the abdominal cavity; other configurations may be evaluated in future work. Gravity was also neglected in the model; its effect on HIPEC delivery and catheter placement could be considered. The effects of heat transfer from the abdomen to the exterior, fluid flow in vasculature, and organs surrounding the abdominal cavity,

including the thoracic cavity and pelvic bones, will also be considered in future work. Thermal heterogeneity would likely be increased due to gravitational forces and additional organs; closed HIPEC procedures have been performed on prostrated patients (10) which would likely reduce fluid flow through posterior regions of the cavity under the catheter placement used here. Other intra-abdominal at-risk locations could be evaluated; the ones in this study were chosen for their clinical relevance. The anatomy of the 3D abdominal cavity and organs, especially the small bowel, was simplified for these simulations and may affect the temperature distribution. Despite this simplification, the results of this study are consistent with (41), which found that HIPEC efficacy reduced and was associated with decreased survival when peritoneal tumors were located on the small bowel. Future 3D cavity and organ design could be informed by anthropometric data and patient-specific CT scans to investigate interpatient heterogeneity and to personalize model predictions. This study contrasted 800 and 1,120 cc/min. However, flow rates as low as 600 cc/min (10) have been reported and could be investigated.

Comparison with similar research

Previous work has developed CFD simulations to study flow in organs and physiological systems (13,17,19,20,22-25). Recently, thermal profiles during HIPEC with flow rates of 1,600–1,800 cc/min in five (upper, mid- and suprapubic) abdominal regions were evaluated with a detailed anatomical model (27), comparing the simulation results to clinically measured data (42) and varying key treatment parameters to evaluate their effect on these profiles. In comparison to previous CFD efforts, our study evaluated flow and temperatures at specific at-risk locations using lower flow rates (800 and 1,120 cc/min). Although higher flow rates have been shown to improve overall abdominal heating during HIPEC (43), lower flow rates (i.e., 600–1,000 cc/min) have seen extensive use (44,45). Furthermore, large volume infusions may be associated with adverse patient outcomes (46,47). The procedure parameters are critical, as complications dependent on these parameters have included gastrointestinal, pulmonary, and hematological events (48), with overall morbidity and mortality rates of 12–60% and 0.9–5.8%, respectively (49).

Explanation of findings

Because cisplatin performance has been shown to improve with increasing temperature from 37 to 43 ℃ (50), thermal heterogeneity in the abdominal cavity could yield uneven therapeutic performance. This suggests that the efficacy of temperature-sensitive chemotherapeutics common to HIPEC may depend on both fluid flow rate and direction of flow, making catheter placement and flow rates an important consideration to reach potentially under-exposed locations where tumor cells may be present. The results further suggest that monitoring outflow temperature may be inadequate for assessing HIPEC performance. Without intra-abdominal temperature monitoring of at-risk locations, it may not be feasible to determine whether target temperatures and temperature homogeneity are being achieved.

Implications and actions needed

The CFD model presented here represents a first step towards designing efficacious tumor targeting during HIPEC. Even with the best combination of cycle parameters tested, several intra-abdominal locations had not yet reached the target temperature by 30 min (*Figure 4*). While longer cycle times are the standard in the U.S. (51), these results raise a concern that achieving acceptable treatment duration of at-risk locations may not be possible without excessively long cycle times. However, the present model tested relatively few cycle parameters based on a standard four-catheter (two inlet and two outlet) circuit as is commonly used with the Belmont pumps, which is the practice at our institution (52). Expanding the capabilities of the model to incorporate new catheter arrangements in addition to the other cycle parameters previously mentioned may allow for designing techniques that produce rapid equilibration of temperature across all at-risk locations, which would also allow for maximizing tissue exposure times while minimizing overall procedure durations.

Conclusions

It may be unfeasible to assess whether target temperatures and temperature homogeneity is being achieved during HIPEC without temperature monitoring at at-risk locations. Monitoring outflow temperature may be insufficient for this purpose. The results of this study demonstrate that computational analysis offers the capability to monitor intra-abdominal locations at-risk of suboptimal heating and fluid flow as a function of HIPEC parameters. In particular, catheter placement and flow rates

are an important consideration to reach potentially under-exposed locations where tumor cells may remain post CRS. This study provides an initial step towards designing efficacious tumor targeting during HIPEC.

Acknowledgments

Authors thank Jacob Sebree and Emma Little for early evaluation of CFD model feasibility.
Funding: None.

Footnote

Data Sharing Statement: Available at https://jgo.amegroups.com/article/view/10.21037/jgo-24-352/dss

Peer Review File: Available at https://jgo.amegroups.com/article/view/10.21037/jgo-24-352/prf

Conflicts of Interest: All authors have completed the ICMJE uniform disclosure form (available at https://jgo.amegroups.com/article/view/10.21037/jgo-24-352/coif). The authors have no conflicts of interest to declare.

Ethical Statement: The authors are accountable for all aspects of the work in ensuring that questions related to the accuracy or integrity of any part of the work are appropriately investigated and resolved.

References

1. Rajeev R, Klooster B, Turaga KK. Impact of surgical volume of centers on post-operative outcomes from cytoreductive surgery and hyperthermic intra-peritoneal chemoperfusion. J Gastrointest Oncol 2016;7:122-8.
2. Gesson-Paute A, Ferron G, Thomas F, et al. Pharmacokinetics of oxaliplatin during open versus laparoscopically assisted heated intraoperative intraperitoneal chemotherapy (HIPEC): an experimental study. Ann Surg Oncol 2008;15:339-44.
3. Armstrong DK, Bundy B, Wenzel L, et al. Intraperitoneal cisplatin and paclitaxel in ovarian cancer. N Engl J Med 2006;354:34-43.
4. Ghirardi V, Trozzi R, Scanu FR, et al. Expanding the Use of HIPEC in Ovarian Cancer at Time of Interval Debulking Surgery to FIGO Stage IV and After 6 Cycles of Neoadjuvant Chemotherapy: A Prospective Analysis on Perioperative and Oncologic Outcomes. Ann Surg Oncol 2024;31:3350-60.
5. Goodman MD, McPartland S, Detelich D, et al. Chemotherapy for intraperitoneal use: a review of hyperthermic intraperitoneal chemotherapy and early post-operative intraperitoneal chemotherapy. J Gastrointest Oncol 2016;7:45-57.
6. Cashin P, Sugarbaker PH. Hyperthermic intraperitoneal chemotherapy (HIPEC) for colorectal and appendiceal peritoneal metastases: lessons learned from PRODIGE 7. J Gastrointest Oncol 2021;12:S120-8.
7. Sugarbaker PH, Yu W, Yonemura Y. Gastrectomy, peritonectomy, and perioperative intraperitoneal chemotherapy: the evolution of treatment strategies for advanced gastric cancer. Semin Surg Oncol 2003;21:233-48.
8. Boutros C, Somasundar P, Espat NJ. Early results on the use of biomaterials as adjuvant to abdominal wall closure following cytoreduction and hyperthermic intraperitoneal chemotherapy. World J Surg Oncol 2010;8:72.
9. Yurttas C, Hoffmann G, Tolios A, et al. Systematic Review of Variations in Hyperthermic Intraperitoneal Chemotherapy (HIPEC) for Peritoneal Metastasis from Colorectal Cancer. J Clin Med 2018;7:567.
10. Ba M, Cui S, Long H, et al. Safety and Effectiveness of High-Precision Hyperthermic Intraperitoneal Perfusion Chemotherapy in Peritoneal Carcinomatosis: A Real-World Study. Front Oncol 2021;11:674915.
11. Ramirez MF, Guerra-Londono JJ, Owusu-Agyemang P, et al. Temperature management during cytoreductive surgery with hyperthermic intraperitoneal chemotherapy. Front Oncol 2023;12:1062158.
12. González-Moreno S, González-Bayón LA, Ortega-Pérez G. Hyperthermic intraperitoneal chemotherapy: Rationale and technique. World J Gastrointest Oncol 2010;2:68-75.
13. Löke DR, Helderman RFCPA, Franken NAP, et al. Simulating drug penetration during hyperthermic intraperitoneal chemotherapy. Drug Deliv 2021;28:145-61.
14. Helderman RFCPA, Löke DR, Kok HP, et al. Variation in Clinical Application of Hyperthermic Intraperitoneal

Chemotherapy: A Review. Cancers (Basel) 2019;11:78.
15. Acs M, Halmy L, Isgandarova S, et al. Hyperthermic Intraperitoneal Chemotherapy With Cisplatin and Doxorubicin for 90 Minutes Versus 60 Minutes After Cytoreductive Surgery (CRS). Does the 30-Minute Difference Matter? A Comparative Study in a High Volume Centre. Anticancer Res 2022;42:1019-29.
16. Acs M, Babucke M, Jusufi M, et al. Current clinical practices of cytoreductive surgery (CRS) and hyperthermic intraperitoneal chemotherapy (HIPEC). Innov Surg Sci 2024;9:3-15.
17. Morris PD, Narracott A, von Tengg-Kobligk H, et al. Computational fluid dynamics modelling in cardiovascular medicine. Heart 2016;102:18-28.
18. Doost SN, Ghista D, Su B, et al. Heart blood flow simulation: a perspective review. Biomed Eng Online 2016;15:101.
19. Soudah E, Ng EY, Loong TH, et al. CFD modelling of abdominal aortic aneurysm on hemodynamic loads using a realistic geometry with CT. Comput Math Methods Med 2013;2013:472564.
20. Sforza DM, Putman CM, Cebral JR. Computational fluid dynamics in brain aneurysms. Int J Numer Method Biomed Eng 2012;28:801-8.
21. Paritala PK, Anbananthan H, Hautaniemi J, et al. Reproducibility of the computational fluid dynamic analysis of a cerebral aneurysm monitored over a decade. Sci Rep 2023;13:219.
22. Ferrua MJ, Singh RP. Modeling the fluid dynamics in a human stomach to gain insight of food digestion. J Food Sci 2010;75:R151-62.
23. Debbaut C, Vierendeels J, Casteleyn C, et al. Perfusion characteristics of the human hepatic microcirculation based on three-dimensional reconstructions and computational fluid dynamic analysis. J Biomech Eng 2012;134:011003.
24. Nowak N, Kakade PP, Annapragada AV. Computational fluid dynamics simulation of airflow and aerosol deposition in human lungs. Ann Biomed Eng 2003;31:374-90.
25. Kasiteropoulou D, Topalidou A, Downe S. A computational fluid dynamics modelling of maternal-fetal heat exchange and blood flow in the umbilical cord. PLoS One 2020;15:e0231997.
26. Steuperaert M, Debbaut C, Carlier C, et al. A 3D CFD model of the interstitial fluid pressure and drug distribution in heterogeneous tumor nodules during intraperitoneal chemotherapy. Drug Deliv 2019;26:404-15.
27. Löke DR, Kok HP, Helderman RFCPA, et al. Application of HIPEC simulations for optimizing treatment delivery strategies. Int J Hyperthermia 2023;40:2218627.
28. van Driel WJ, Koole SN, Sikorska K, et al. Hyperthermic Intraperitoneal Chemotherapy in Ovarian Cancer. N Engl J Med 2018;378:230-40.
29. Valle SJ, Alzahrani NA, Liauw W, et al. Hyperthermic Intraperitoneal Chemotherapy (HIPEC) Methodology, Drugs and Bidirectional Chemotherapy. Indian J Surg Oncol 2016;7:152-9.
30. Wang WY, Wu MF, Wu DB, et al. Calculating the dose of cisplatin that is actually utilized in hyperthermic intraperitoneal chemotherapy among ovarian cancer patients. J Ovarian Res 2021;14:9.
31. Friis SJ, Hansen TS, Poulsen M, et al. Biomechanical properties of the stomach: A comprehensive comparative analysis of human and porcine gastric tissue. J Mech Behav Biomed Mater 2023;138:105614.
32. Hasgall PA, Di Gennaro F, Baumgartner C, et al. IT'IS database for thermal and electromagnetic parameters of biological tissues, 2018. Available online: www.itis.ethz.ch/database
33. Blinzler BJ, Khalili P, Ahlström J. Integrated Computational Material Design for PMC Manufacturing with Trapped Rubber. Materials (Basel) 2020;13:3825.
34. Ansys Fluent Theory Guide: Ansys, Inc. Availab;e online: https://www.ansys.com/
35. Ansys® Academic Research Fluids, Help System, Ansys Fluent User's Guide: Ansys, Inc. Availab;e online: https://www.ansys.com/
36. Parissis P, Romeos A, Giannadakis A, et al. Computational Study of Hemodynamic Field of an Occluded Artery Model with Anastomosis. Bioengineering (Basel) 2023;10:146.
37. Díaz M, Becker DE. Thermoregulation: physiological and clinical considerations during sedation and general anesthesia. Anesth Prog 2010;57:25-32; quiz 33-4.
38. Kusamura S, Dominique E, Baratti D, et al. Drugs, carrier solutions and temperature in hyperthermic intraperitoneal chemotherapy. J Surg Oncol 2008;98:247-52.
39. Helderman RFCPA, Löke DR, Verhoeff J, et al. The Temperature-Dependent Effectiveness of Platinum-Based Drugs Mitomycin-C and 5-FU during Hyperthermic Intraperitoneal Chemotherapy (HIPEC) in Colorectal Cancer Cell Lines. Cells 2020;9:1775.
40. Schaaf L, van der Kuip H, Zopf W, et al. A Temperature of 40 °C Appears to be a Critical Threshold for Potentiating Cytotoxic Chemotherapy In Vitro and in Peritoneal Carcinomatosis Patients Undergoing HIPEC. Ann Surg Oncol 2015;22 Suppl 3:S758-65.

41. Wong JSM, Tan GHC, Cheok SHX, et al. Implications of peritoneal cancer index distribution on patients undergoing cytoreductive surgery and hyperthermic intraperitoneal chemotherapy. Pleura Peritoneum 2022;7:95-102.
42. Rettenmaier MA, Mendivil AA, Gray CM, et al. Intra-abdominal temperature distribution during consolidation hyperthermic intraperitoneal chemotherapy with carboplatin in the treatment of advanced stage ovarian carcinoma. Int J Hyperthermia 2015;31:396-402.
43. Furman MJ, Picotte RJ, Wante MJ, et al. Higher flow rates improve heating during hyperthermic intraperitoneal chemoperfusion. J Surg Oncol 2014;110:970-5.
44. Batista TP, Badiglian Filho L, Leão CS. Exploring flow rate selection in HIPEC procedures. Rev Col Bras Cir 2016;43:476-9.
45. Neveu J, Tremblay E, Mercier F, et al. Developing a hyperthermic intraperitoneal chemotherapy (HIPEC) gynecologic oncology program: a Canadian experience. Int J Gynecol Cancer 2023;33:1957-65.
46. Eng OS, Dumitra S, O'Leary M, et al. Association of Fluid Administration With Morbidity in Cytoreductive Surgery With Hyperthermic Intraperitoneal Chemotherapy. JAMA Surg 2017;152:1156-60.
47. Peng JS, LaPiano J, Wang K, et al. Restrictive Intraoperative Fluid Rate is Associated with Improved Outcomes in Cytoreductive Surgery and Hyperthermic Intraperitoneal Chemotherapy. Ann Surg Oncol 2022;29:163-73.
48. Mehta SS, Gelli M, Agarwal D, et al. Complications of Cytoreductive Surgery and HIPEC in the Treatment of Peritoneal Metastases. Indian J Surg Oncol 2016;7:225-9.
49. Wajekar AS, Solanki SL, Patil VP. Postoperative complications and critical care management after cytoreduction surgery and hyperthermic intraperitoneal chemotherapy: A systematic review of the literature. World J Crit Care Med 2022;11:375-86.
50. Los G, van Vugt MJ, den Engelse L, et al. Effects of temperature on the interaction of cisplatin and carboplatin with cellular DNA. Biochem Pharmacol 1993;46:1229-37.
51. Turaga K, Levine E, Barone R, et al. Consensus guidelines from The American Society of Peritoneal Surface Malignancies on standardizing the delivery of hyperthermic intraperitoneal chemotherapy (HIPEC) in colorectal cancer patients in the United States. Ann Surg Oncol 2014;21:1501-5.
52. Riley W. Belmont Hyperthermia Pump in the conduct of intra-operative heated chemotherapy. Perfusion 2009;24:115-8.

Cite this article as: Cooney OS, Goodin DA, Mouw TJ, Martin RCG, Frieboes HB. Intra-abdominal temperature variation during hyperthermic intraperitoneal chemotherapy evaluated via computational fluid dynamics modeling. J Gastrointest Oncol 2024;15(4):1847-1860. doi: 10.21037/jgo-24-352

